BIOCELL
2021 45(6): 1569-1583

Tech Science Press

Repurposing of FDA-Approved drugs to predict new inhibitors against key regulatory genes in *Mycobacterium tuberculosis*

Xinjun YANG[1]; Aftab ALAM[2]; Naiyar IQBAL[3]; Khalid RAZA[4,*]

[1] Department of Pediatrics, 3201 Hospital, Hanzhong, China
[2] Centre for Interdisciplinary Research in Basic Sciences, Jamia Millia Islamia, New Delhi, India
[3] Department of Computer Science and Information Technology, Maulana Azad National Urdu University, Hyderabad, India
[4] Department of Computer Science, Jamia Millia Islamia, New Delhi, India

Key words: Virtual screening, Molecular docking, MD simulation, PPI network

Abstract: Tuberculosis (TB) disease has become one of the major public health concerns globally, especially in developing countries. Numerous research studies have already been carried out for TB, but we are still struggling for a complete and quick cure for it. The progress of *Mycobacterium tuberculosis* (MTB) strains resistant to existing drugs makes its cure and control very complicated. Therefore, it is the need of the hour to search for newer and effective drugs that can inhibit an increasing number of putative drug targets. We applied the drug repurposing concept to identify promising FDA-approved drugs against five key-regulatory genes (FurB, IdeR, KstR, MosR, and RegX3) of the MTB. The FDA drugs were virtually screened using a structure-based approach by GOLD versions 5.2, and subjected to rigid docking followed by an induced-fit docking algorithm to enhance the accuracy and prioritize drugs for repurposing. We found 11 candidate drugs (including ZINC03871613, ZINC03871614, ZINC03871615 as top scorer candidate drugs) that were frequently present within the top 20 GoldScore ranks and showed promising results. Furthermore, molecular dynamics simulation was performed to monitor the effect of the top scorer drugs on the structural stability of all the five targets, indicating that inhibitors preferentially bind to the active site of the targets. This work suggests that these known FDA-approved drugs open new application domains in the form of anti-tuberculosis agents.

Introduction

Tuberculosis (TB) is one of the oldest diseases with molecular evidence that dates back to17,000 years ago. Despite advances in modalities for diagnosis and treatment of TB, unfortunately, people are still suffering, and it is among the top 10 killer communicable diseases worldwide, second only to HIV. TB is a communicable disease caused by *Mycobacterium tuberculosis*. It typically affects the lungs (pulmonary TB) but can affect other sites as well (extra-pulmonary TB) (Ahmad, 2011). The disease is spread in the air when people who are sick with pulmonary diseases expel bacteria during coughing. According to WHO, six countries hold 60% of all the TB burden of the entire world in which India is the leading country followed by Indonesia, China, Nigeria, Pakistan, and South Africa (shown in Fig. 1). The Central TB Division, Ministry of Health and Family Welfare, India has published a report on "India TB report 2018" which reported TB statistics for India for 2016 to give an estimated incidence figure of 2.79 million cases of TB for India and up to 4.23 lakh patients were estimated to have died during the year (India TB Report, 2018). Multidrug-resistant (MDR) tuberculosis (TB) is a serious global public health problem (Dua *et al.*, 2018), and estimates indicate that unless the management of MDR TB changes radically, it will be one of the main drivers of antimicrobial resistance, which could kill more persons than cancer by 2050 (Ho *et al.*, 2016). Major challenges to curb the TB in India include poor primary healthcare system in rural areas, unregulated private health care leading to the indiscriminate use of first-line and second-line anti-TB drugs, spreading HIV infection, poverty, and lack of administrative coordination among government bodies responsible for health and hygiene (Singh *et al.*, 2017). Hence, there is an urgent need to design or developed nontoxic biocompatible drugs against TB (Peters *et al.*, 2020; Weiner *et al.*, 2020).

In our study, we have used the drug repurposing concept, which is a method for disease cure that accelerates the identification of new uses for existing drugs with minimum

*Address correspondence to: Khalid Raza, kraza@jmi.ac.in
Received: 21 April 2021; Accepted: 25 May 2021

Doi: 10.32604/biocell.2021.017019

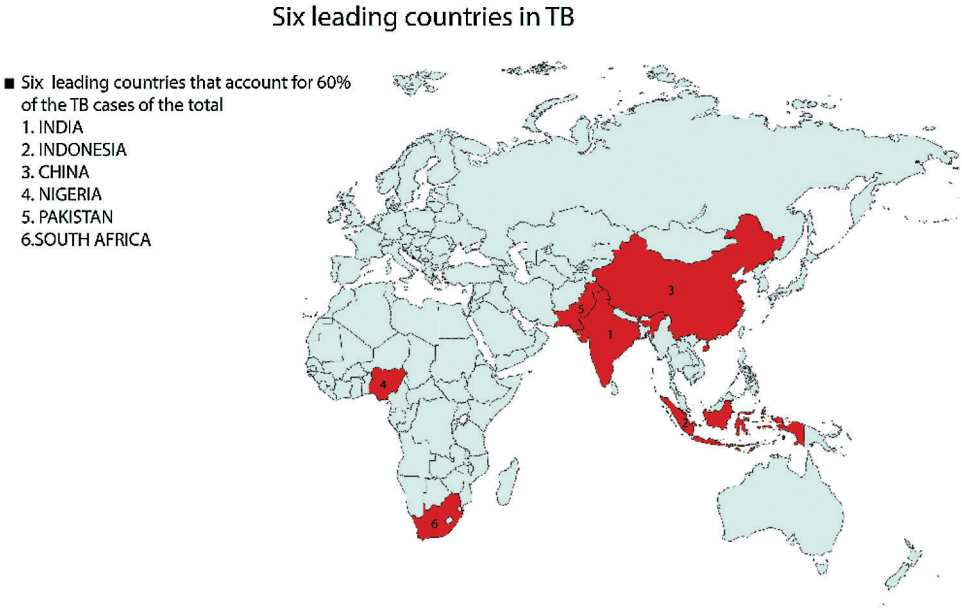

FIGURE 1. Six leading countries account for 60% of the total, with India leading the count, followed by Indonesia, China, Nigeria, Pakistan, and South Africa (WHO).

side effects (Karaman and Sippl, 2019; Lanza *et al.*, 2018; Savoia, 2016). Previous research has shown that the drug repurposing concept (a combination of virtual screening with docking and dynamics studies) can be successfully applied to treat new diseases with existing drugs. For example, the drug sildenafil, which was initially designed for the treatment of hypertension and ischemic heart disease, was later approved for the treatment of erectile dysfunction, representing a successful history of drug repurposing (Afzal *et al.*, 2014; Karthick and Ramanathan, 2013; Li *et al.*, 2001; Palos *et al.*, 2017). Here, we use a computer-guided drug repurposing method and apply it to virtually screened FDA approved drugs against five key regulatory proteins from MTB: (a) FurB–as shown by the regulatory profiles, furB gene is up-regulated in macrophages-phagocytosed bacteria, fascinating that it might be involved in the regulation of intracellular gene expressions. The furB gene is co-transcribed with its upstream gene (Rv2358), which encodes another zinc-dependent regulator and responsible for repressing at least 32 genes, several of which have been implicated with zinc homeostasis. In addition, FurB controls five genes encoding ribosomal proteins three of which containing a putative zinc-binding motif. Based on comparative genomics data these ribosomal proteins have also been suggested to be involved in zinc homeostasis (Lucarelli *et al.*, 2007; Panina *et al.*, 2003). (b) IdeR–It is an iron-dependent regulator that maintains a moderate level of iron inside a bacterium by controlling the transcription of genes, including the expression of its own gene involved in iron uptake, transport, and storage (Banerjee *et al.*, 2011). In *M. tuberculosis* regulation of the intracellular levels of iron are performed by the transcription factor IdeR.In the iron sufficient stage in MTB, iron binds and activates intracellular IdeR, which then represses the iron acquisition machinery of the pathogen and activates the synthesis of iron storage proteins. IdeR also plays a key role in protecting the cells against the oxidative stress generated by the host (Rohilla *et al.*, 2017). (c) KstR–It is a highly conserved *TetR* family transcriptional repressor (TFR) that regulates 78 genes responsible for cholesterol catabolism in MTB (Kendall *et al.*, 2010; Sanz *et al.*, 2011). In MTB, a highly critical enzyme known as 3-β HSO(EC 1.1.1.145) has been primarily involved in the degradation of cholesterol, which transforms cholesterol into cholestenone, In fact, this enzyme is expressed in a cholesterol-independent manner suggesting its availability in the pathogen at any time (García *et al.*, 2012). (d) MosR–This is a highly connected protein in the transcriptional regulatory (TR) network of MTB, one of its functions is to regulate around 295 genes at the level of transcription. The main role of MosR is to up-regulate expression of rv1050 (a putative exported oxidoreductase that has not yet been characterized) in response to oxidants and propose that it is through this role that MosR contributes to the bacterium survival in the macrophage (Brugarolas *et al.*, 2012). (e) RegX3–It is a self-regulatory protein and controls the expression of its own gene. Many RegX3-dependent genes have a role in the biosynthesis of DNA, RNA and other macromolecules (Pei *et al.*, 2021). Whereas, a number of genes participate in the catabolism of fatty acids and are repressed by fadE6, fadE14 and accD2 genes in a direct way (Ahmad and Kumar, 2016; Carroll *et al.*, 2011). This two component system is also responsible for cell wall biosynthesis, lipid biosynthesis and cell envelope protein synthesis (Almatar *et al.*, 2017; Roberts *et al.*, 2011).

Materials and Methods

Preparation of drug target and drug-library

In our study, we considered five key regulatory genes from MTB; *FurB*(PDB ID: 2O03) (Lucarelli *et al.*, 2007), *IdeR* (PDB ID: 1B1B) (Pohl *et al.*, 1999), *KstR* (PDB ID: 3MNL) (Ho *et al.*, 2016), *MosR* (PDB ID: 4FX0) (Brugarolas *et al.*, 2012) and *RegX3* (PDB ID: 2OQR) (King-Scott *et al.*, 2007), details are given in Fig. 2. All the atomic coordinates (x-ray structure with good resolution, from 1.8Å to 2.7Å) of these proteins were downloaded from Protein Data Bank (Berman *et al.*, 2000). The proteins were optimized for docking by

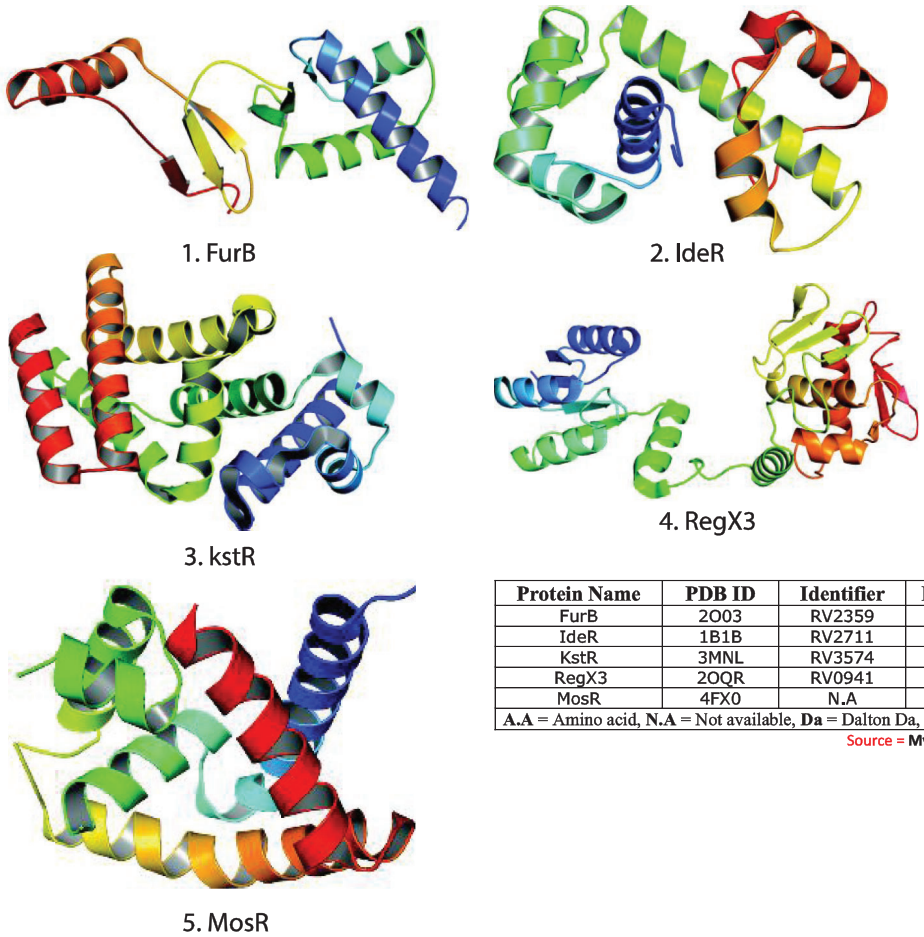

Protein Name	PDB ID	Identifier	Length	M. Mass (D.a)	PI
FurB	2O03	RV2359	130 AA	14397.9	6.338
IdeR	1B1B	RV2711	230 AA	25232.9	5.046
KstR	3MNL	RV3574	199 AA	21935.1	9.409
RegX3	2OQR	RV0941	227 AA	24849.4	4.580
MosR	4FX0	N.A	148 AA	15980.0	N.A

A.A = Amino acid, **N.A** = Not available, **Da** = Dalton Da, **PI** = Isoelectric point

Source = **Mycobrowser** (https://mycobrowser.epfl.ch/)

FIGURE 2. Key regulatory genes from MTB. FurB (PDB ID: 2O03), IdeR (PDB ID: 1B1B), KstR (PDB ID: 3MNL), MosR (PDB ID: 4FX0) and RegX3 (PDB ID: 2OQR).

following standard procedures, which include removal of crystallographic water molecules, the addition of missing H-atoms, and minimizing the energy level of all the proteins using the Swiss-PDB viewer tool and this server provides an energy minimization facility using the GROMOS96 force field (Alam *et al.*, 2016; Johansson *et al.*, 2012). All the targets were further refined using SCWRL 4.0 tool to minimize side-chain to backbone clashes and the side-chain-to-side chain clashes (Wang *et al.*, 2008). The drug library consists of 1985 drugs (FDA approved) which were downloaded from the ZINC-15database (Irwin *et al.*, 2012). CORINA Classic (the classic command-line version of CORINA) (https://www.mn-am.com/products/corina) was used to prepare the drug-library because it facilitates preparation of high quality, low energy, single, 3D structure with correct chirality.

Virtual screening

Virtual screening (VS) is a computational method used in drug designing and discovery to find out the series of (compound library) small molecules in order to identify the most potent molecules which are most likely to bind to a drug target (Krueger *et al.*, 2016; Morrone Xavier *et al.*, 2016; Rester, 2008; Rollinger *et al.*, 2008). In our study, VS was performed by using GOLD versions 5.2 (Genetic Optimisation for Ligand Docking; Cambridge Crystallographic Data Centre) (Jones *et al.*, 1995; Jones *et al.*, 1997). GOLD uses genetic algorithms to dock ligand with the receptor. The scoring function "GoldScore" was tested individually for each protein. The molecular docking that utilizes the genetic algorithm (GA) was set to three different execution runs–(a) 50, (b) 100, and (c) 200 GA runs, so as to identify influential and high-affinity binding modes. The radius of the docking sphere was 10–12 Å centered at the position, a maximum of 100,000 operations were performed that deliver high prediction accuracy but are relatively slow (Heberlé and De Azevedo, 2011; Potemkin and Grishina, 2018). The information on the binding site for all the targets was observed from the available literature which was then used further for grid generation. For *FurB* and *IdeR*, we used its active repressor site (Lucarelli *et al.*, 2007) for *KstR* and *MosR*, we used its DNA binding site (Brugarolas *et al.*, 2012; Ho *et al.*, 2016) and for *RegX3*, we used its conformational switch region (present 'hotspot' residues) (Ahmad *et al.*, 2015; Khalid *et al.*, 2018).

Molecular dynamics study

As we are aware of the remarkable biological functions of proteins and DNA and also their profound dynamic mechanisms which include switching between active and inactive states (Autiero *et al.*, 2013), cooperative effects the intercalation of drugs into DNA (Chou and Mao, 1988), and allosteric transition (Ward *et al.*, 2010) can be unveiled by studying their internal motions (Lin and Lapointe, 2013).

Likewise, to understand the action mechanism of receptor-ligand binding, we should not consider only the static structures concerned, but also the dynamical information obtained by simulating their internal motions or dynamic processes (de Azevedo, Jr *et al.*, 2001; de Azevedo, 2011; Qazi and Raza, 2021). To realize this, initially, MD Simulations were performed for proteins only, e.g., *FurB*, *IdeR*, *KstR*, *RegX3*, and *MosR*at 300K to investigate the stability profile. We observed that drug ZINC03871613 was best docked with the three targets (FurB, KstR, and RegX3), and drugs ZINC03871615, ZINC03871614 were docked with MosR and IdeR targets, respectively. These are the best candidate drugs that exhibit high binding affinity with the targets. To observe conformational changes due to the presence of ligands in the active site, we performed MD simulations for protein complexes too.

Molecular dynamics (MD) simulations were performed using the GROMACS version 5.1 software (van der Spoel *et al.*, 2005) with the standard GROMOS 53*A*6 force field was used. The proteins were soaked in a cubic box of water molecules with a dimension of 10 Å, i.e., setting the box edge 10 Å from the molecule perimeters, using the *editconf* module for making boundary conditions and *genbox* for solvation. For the solvation of proteins, the *spc*216 template was used. The charges of the complete system are neutralized by the addition of Na^+ and Cl^- ions (if the system has a positive charge (e.g., +6), add 6 Cl^- ions and if the system has a negative charge (e.g., −6), add 6 Na^+ ions)) using the *gmxgenion* module to maintain neutrality. The system was then minimized using the 1500 steps of steepest descent at 300K during their equilibration period (100 ps) at a constant volume under periodic boundary conditions. Equilibration was performed in two phases: NVT ensemble (constant number of particles, volume, and temperature at 100 ps) and NPT ensemble (constant number of particles, pressure, and temperature at 100 ps). After the equilibration phase, the particle *MeshEwald* method (Cheatham *et al.*, 1995) was used. Production phases were performed at 300K. The resulting trajectories were analyzed, using RMSD, RMSF, RG, and SASA by the utilities provided by GROMACS. For ligand topology, we used SWISSPARAM that provides topologies and parameters for small organic molecules, compatible with the CHARMM all atoms force field, for use with the CHARMM or GROMACS software (Bjelkmar *et al.*, 2010; Zoete *et al.*, 2011). The server is fully automatic, and we only need to provide the drug molecule in the mol2 format.

Protein–Protein interaction network

The protein-protein interaction (PPI) networks are much important for the system-level understanding of cellular processes (Cau *et al.*, 2018). Such networks are used for screening and evaluation of functional genomics data and provide an instinctive platform for annotating structural, functional, and evolutionary properties of proteins. The five proteins (*FurB, IdeR, KstR, RegX3, and MosR*) were taken as seed proteins from which we obtained direct and indirect PPIs using theSTRING 10.5 database (Snel *et al.*, 2000). This database provides details on both predicted and experimentally verified interactions from different sources based on their neighborhood, co-occurrence, co-expression, gene fusions, experiments, and literature mining. We constructed a PPI network based on high confidence interaction which means that only interactions with a high level of confidence are considered as potential associations in the PPI network.

Results

Virtual screening

In the first step, the library of FDA approved drugs were screened using GOLD versions 5.2 server. Dock runs of all 1985 drugs on targets namely "FurB (binding cavity: *His-81*, *His-83*, *Cys-76*, *Glu-78*, *Asp-24*, *Asp-62*, etc.), IdeR (binding cavity: *Glu-20*, *Asp-17*, *Arg-80*, etc.), KstR (binding cavity: *Arg-174*, *Glu-112*, *Pro-108*, *Trp-17*, etc.), RegX3 (binding cavity: *Pro-102*, *Tyr-103*, *Ser-104*, etc.) and MosR (binding cavity: *Thr-36*, *His-287*, *Glu-244*, etc.)" using GOLD suite (with 50 GA runs were performed) resulted in a few best candidate drugs evaluated based on the Gold fitness score $\geq$ 55 (The fitness score >50 is supposed to good binding).

We found a total of 828 drugs that were bound with all the targets like FurB, IdeR, KstR, MosR, and RegX3 that were docked with 111, 355, 193, 157, and 12 drugs out of 1985, respectively. In the second step, the genetic search algorithm was initially set to 100 then 200 GA runs for 828 drugs to each target and in most cases, similar results were obtained. The docking and scoring details are shown in Fig. 3 and Suppl. Tab. S1. In the third step, we again filtered out the drugs that frequently bounded with all the targets at set threshold among the top 20 GoldScore ranks. It was found that only 11 candidate drugs (designated with Zinc Database ids as *ZINC03871612, ZINC03871613*, *ZINC03871614*, *ZINC03871615*, *ZINC01529323*, *ZINC03830426*, ZINC03830428, *ZINC03830430, ZINC03830635, ZINC03799072*, and *ZINC08551107)* are consistently binding with all the targets.

The consistent binding idea was given preference for the selected 11 candidate drugs over top 20 (for each target) as a matter of feasibility towards *in-vitro* or *in-vivo* testing for these bindings. The 2D structures of these 11 candidate drugs can be obtained from the ZINC-15 database (https://zinc15.docking.org/). In this study, we have visualized only top-ranked candidate drugs which are best bound with the targets like *FurB*, *KstR*, and *RegX3*, are docked with *ZINC03871613*, while *IdeR* and *MosR* are docked with *ZINC03871614*, and *ZINC03871615* with GoldScore 77.58, 75.02, 62.54, 81.69, and 79.72, respectively. While studying the docked conformation of the FurB complex, mainly the three residues, ASP-24, GLU-78, and HIS-81 were found to form H-bonds with the ligands in the docked complex along with 12 surrounding residues. As in the case of KstR and RegX3 complexes, ASP-82, PRO-102, SER-104, and LYS-157 (also forms salt bridge interaction) and the residues LEU-109, ARG-174 (also forms π–π and π-cation and salt bridge interactions) make H-bond with the ligand along with 14 and eight surrounding residues, respectively. While in the case of the MosR complex, the residues, ARG-20 (also make π–π and π-cation interaction), ASP-27, THR-36, ASN-37, THR-38, ARG-75 (also forms salt bridge interaction), and ASN-76 while in the IdeR complex, the residues ARG-13,

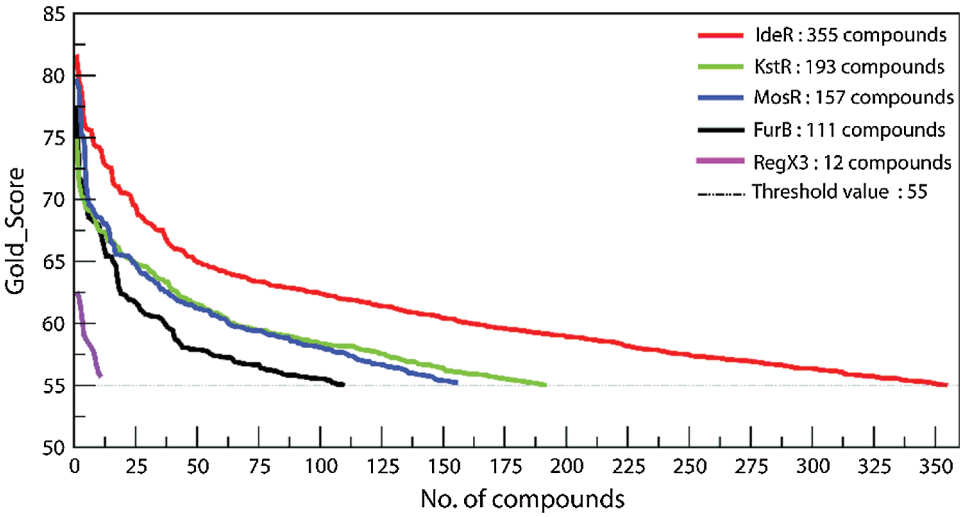

FIGURE 3. The plot represents the Gold Score of compounds that have scored equal, or above the threshold value of 55.0. (A) IdeR bind with 355 compounds (B) KstR bind with 193 compounds (C) MosR bind with 157 compounds (D) FurB bind with 111 compounds (E) RegX3 bind with 12 compounds.

ARG 33, ARG-80 (also make π–π interaction) were seemed to make H-bonds with the ligands along with six and 17 surrounding residues, respectively. The complete details are given in Fig. 4 and Tab. 1. All the top scorer candidate drugs are purine derivatives in the form of triphosphate and the basic difference among them is in the cyclic pyranose which are isomers of each other due to the different spatial orientation of the hydroxyl group.

MD simulation analysis

We performed MD simulation at 300K of the protein-ligand complex with top-ranked drugs to observe the effect on the structure, behavior, and flexibility of all the targets. We analyzed the RMSD, RMSF, RG, and SASA for all the selected targets, as shown in Fig. 5.

Stability of the trajectory

a) Root-mean-square deviations (RMSD) from the native structure coordinates during the MD simulation were used to assess the stability and the reliability of the simulation. In our study, we noticed that *FurB* underwent structural fluctuations starting from the first 5 *ns* of the trajectory, although the amplitude of the fluctuation was smaller for the FurB complex at 6.44 *ns*, a slight transition of 0.325 *nm* was spotted and the system got optimized after 8 *ns* at 0.65 *nm*. This significant drift in RMSD of 0.325 *nm* is verified by the protein-ligand interactions within the complex. However, the simulation ends with a total drift of 0.28 *nm* from the native structure. A significant drift in RMSD of *FurB* and *FurB complex* indicate the conformational change in the receptor that has occurred to fit the ligand in the active site of the FurB.

b) In the case of the *IdeR*, the trajectory (RMSD) remains stable throughout the simulation with small drifts, but the fluctuations were smaller too for the *IdeR complex*, up to 7.15 *ns*. At the three points, a gradual transition of 0.083, 0.096, and 0.15 *nm* were observed at 0.24, 2.54 *and* 5.91 *ns*, respectively and after 11 *ns*, the trajectory was optimized. These significant drifts are verified by the protein-ligand interactions within the complex.

c) In the case of the*RegX3*, the trajectory (RMSD) drastically fluctuated with large drifts, but the fluctuations were smaller for the *RegX3 complex*. A gradual transition of 1.056 *nm* at 4.06 *ns* was observed in the native structure, but the system is optimized after 12 *ns*. A significant difference in RMSD of RegX3 and complex strongly indicates a conformational change in the protein due to ligand.

d) In the case of the *MosR*, the trajectory (RMSD) drastically fluctuated with large drifts, but the fluctuations were smaller for the *MosR complex*. A drastic transition of 0.5064 *nm* at 1.07 *ns* was observed in the native structure, but later system is optimized after 3.5 *ns*. However, the simulation ends with a total drift of 0.249 *nm* from the native structure, and this difference in RMSD indicates the conformational changes in the protein due to ligand.

e) In the case of the *KstR*, the trajectory (RMSD) remains stable throughout the simulation with small drifts of 0.103 *nm*, but the fluctuation pattern was slightly different from the *kstR complex*, a drastic transition of 0.287 *nm* is observed but the system is optimized after 8.6 ns. The average total drift in RMSD at the end of both simulations was 0.192 *nm*. This difference in RMSD of *kstR* and *kstR complex* indicates a conformational change in the protein due to ligand.

The root mean square fluctuation (RMSF)

a) We have performed RMSF from its time-averaged position to set up the conformational fluctuations of the *FurB* and *FurB* complex at the residual level. The average residual fluctuation of all the residues in the case of *FurB complex* is lower than *FurB*. These results suggest that the α-helical structure of *FurB* is more specifically maintained due to the binding of the ligand.

b) RMSF analysis for the *IdeR* revealed that fluctuation of amino acids was largest in the region from 33–41 residues in *IdeR*, but in the case of *IdeR complex*, residues *V56, A57, G58*, and *D59* have a greater RMSF score. The region 61–80 residues slightly fluctuated up and down in both cases (complex and protein), which confirms the important role being played by these residues in the ligand-binding process.

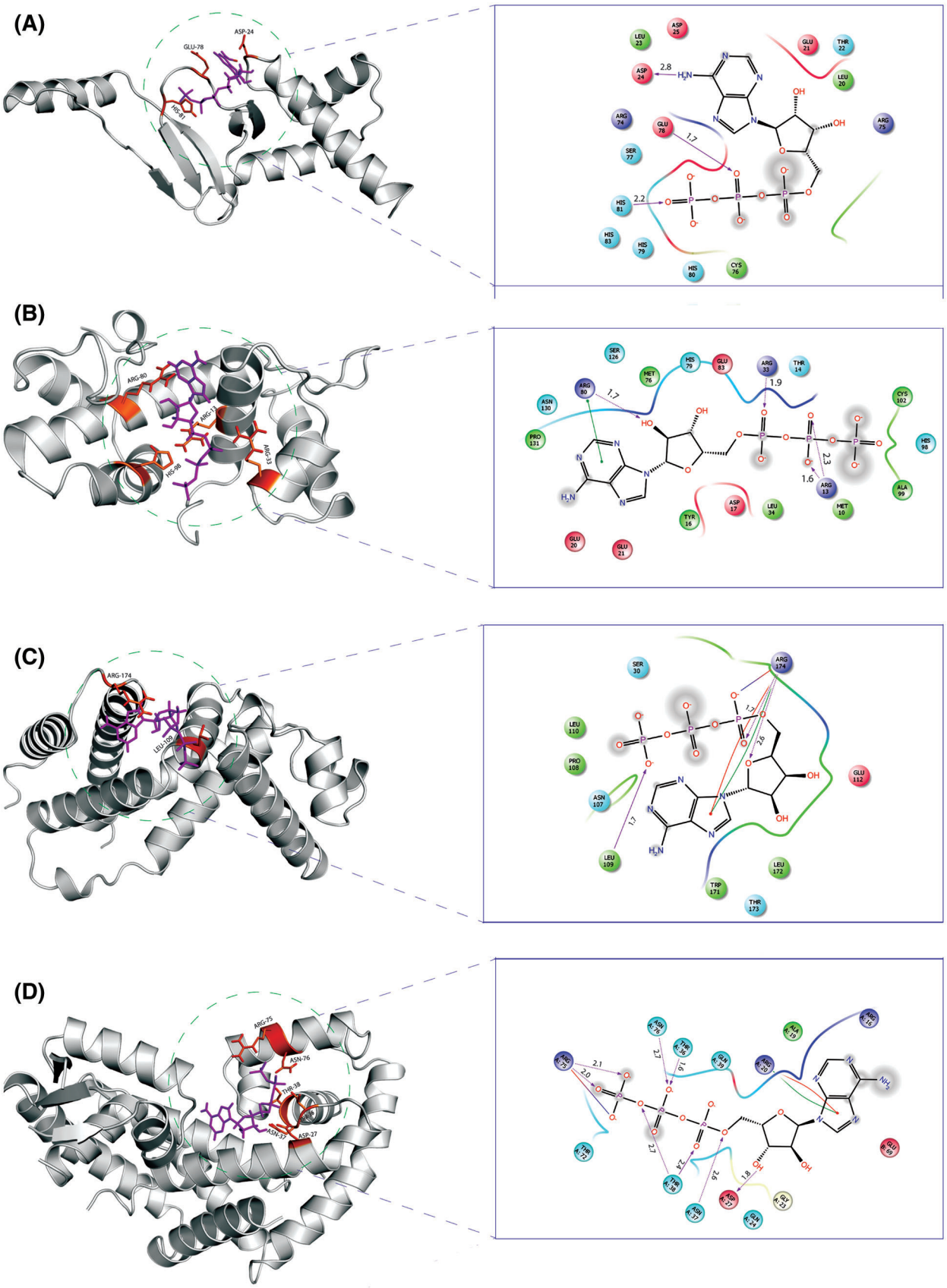

FIGURE 4. (continued)

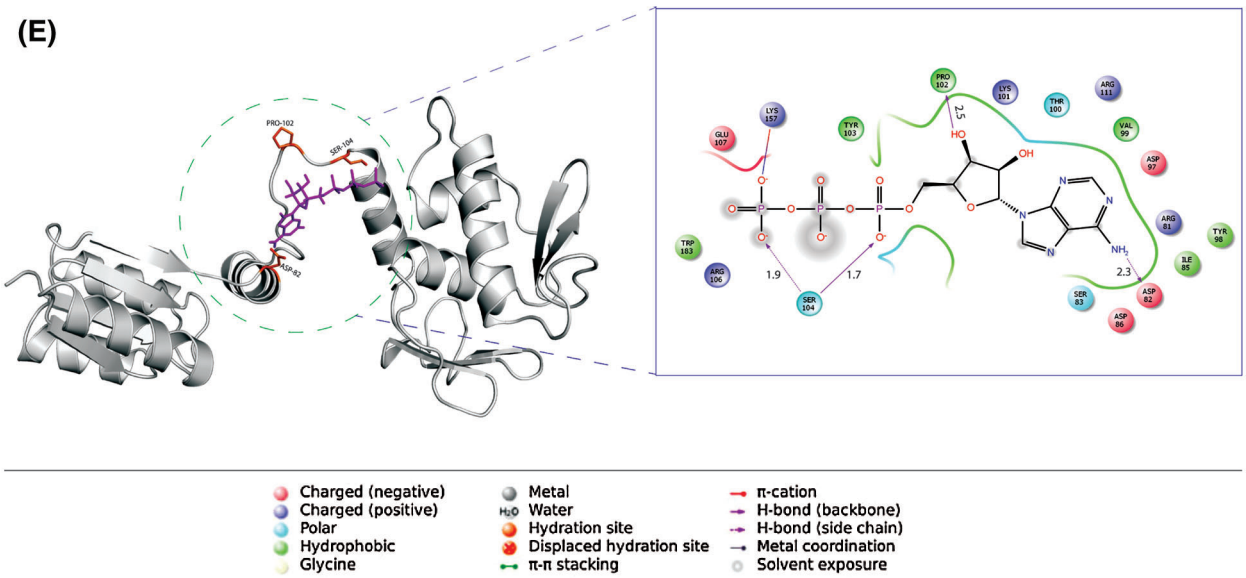

FIGURE 4. Binding poses are suggested by molecular docking. (A) Molecular docking poses of compound ZINC03871613 with FurB. (B) Compound ZINC03871614 docked with IdeR. (C) Compound ZINC03871613 docked with KstR. (D) Compound ZINC03871615 docked with MosR. (E) Compound ZINC03871613 docked with RegX3. The 2D depiction of the binding pocket and interactions are generated using Maestro with a 4.0 Å cutoff. Protein residues forming hydrogen bonds are indicated with two different magenta lines (i) solid lines (backbone) (ii) dashes lines (side chain). The π-π stacking interaction between residues and the aromatic ring of the ligand is shown in the green solid line while π-Cation is a non-covalent molecular interaction is shown in the red solid line.

TABLE 1

Important interaction between the active residues with the various ligands under study upon docking (enclosed in brackets are residues forming H-bonds and underlined residues are showing other interactions)

Protein	Ligand	Gold score	No. of H-bonds	Other interactions	Contact residues	Surrounding residues
FurB (2O03)	*ZINC*03871613	77.58	03	• Polar • Hydrophobic	(ASP-24), (GLU-78), (HIS-81)	LEU-20, GLU-21, THR-22, LEU-23, ASP-25, ARG-74, ARG-75, CYS-76, SER-77, HIS-79, HIS-80, HIS-83
IdeR (1B1B)	*ZINC*03871614	81.69	04	• Polar • π –π stacking • Hydrophobic	(ARG-13), (ARG 33), (ARG-80)	MET-10, THR-14, TYR-16, ASP-17, GLU-20, GLU-21, ARG-33, LEU-34, MET-76, HIS-79, GLU-83, HIS-98, ALA-99, CYS-102, SER-126, ASN-130, PRO-131
KstR (3MNL)	*ZINC*03871613	75.02	03	• Polar • π –π stacking • π – Cation • Salt bridge • Hydrophobic	(LEU-109), (ARG-174)	SER-30, ASN-107, PRO-108, LEU-110, GLU-112, TRP 171, LEU-172, THR-173
MosR (4FX0)	*ZINC*03871615	79.77	08	• Polar • π –π stacking • π – Cation • Salt bridge • Hydrophobic	ARG-20, (ASP-27), (THR-36), (ASN-37), (THR-38), (ARG-75), (ASN-76)	ARG-16, ALA-19, GLY-23, GLN-24, GLN-39, THR-72
RegX3 (2OQR)	*ZINC*03871613	62.54	04	• Polar • Salt bridge • Hydrophobic	(ASP-82), (PRO-102), (SER-104), LYS-157	ARG-81, TRP-83, ILE-85, ASP-86, ASP-97, TYR-98, VAL-99, THR-100, LYS-101, TYR-103, ARG-106, GLU-107, ARG-111, TRP-183

c) On analyzing the fluctuations in the *RegX3* and *RegX3 complex*, it was observed that fluctuation of amino acids was the largest in the two regions, 80–89 and 91–114 residues in both cases due to the presence of the active site in this region, which confirms the important role being played by these residues in ligand binding.

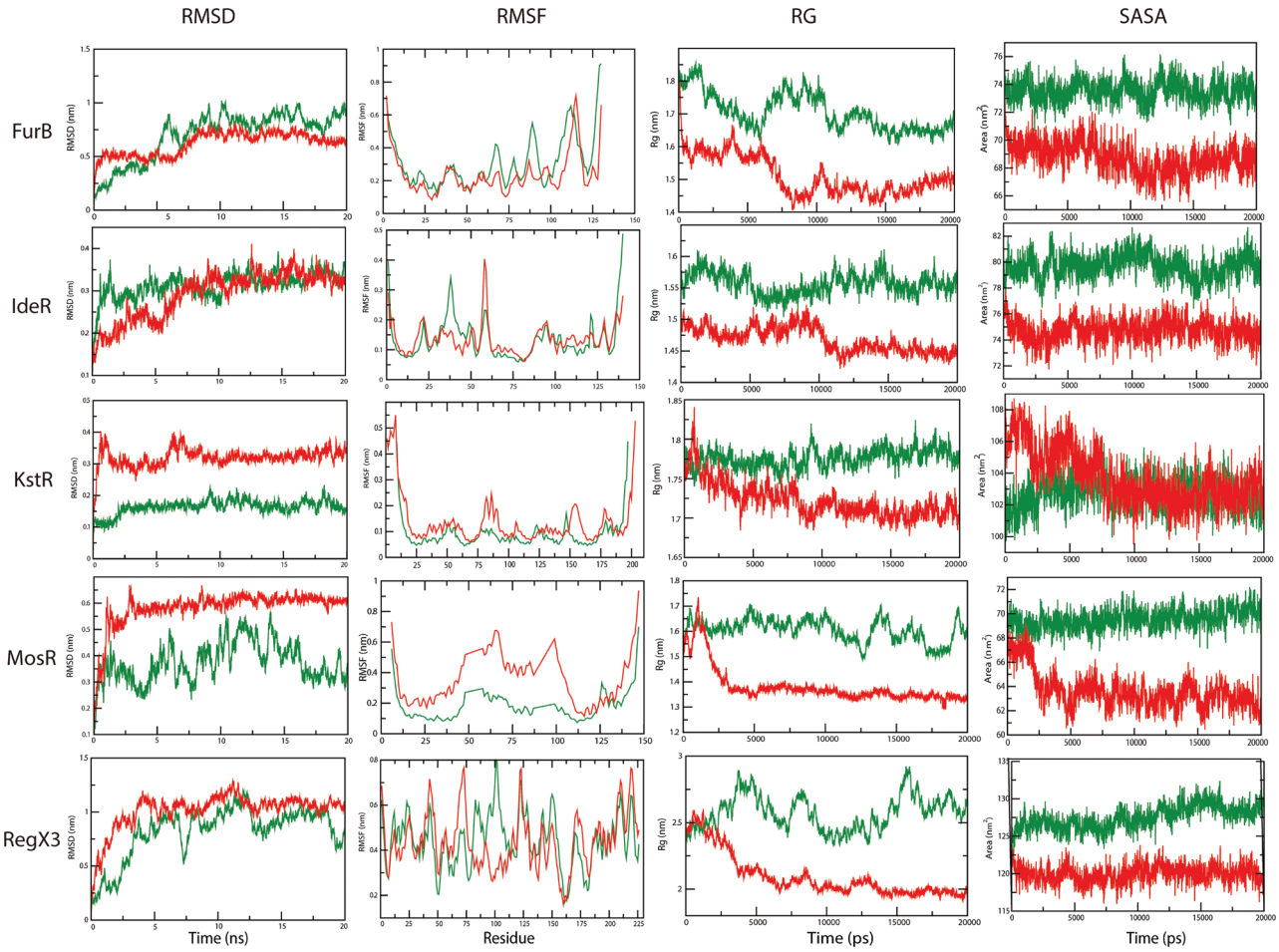

FIGURE 5. Molecular dynamics study. In this figure, we have shown RMSD, RMSF, RG, and SASA values each at 300k for our all targets (FurB, IdeR, KstR, MosR, and RegX3). The target protein and the complex (protein with ligands) are shown in green and red color, respectively.

d) In RMSF analysis of theMosR, we observed that fluctuation of amino acids was largest in the two regions from 14–40 and 44–110 residues, in both *MosR* and *mosR complex*. The First fluctuation (between 14–40 residues) was started due to the presence of an active site where the ligand binds, and the second fluctuation occurred due to residual conformational changes in MosR protein.

e) The fluctuations of KstR are less than *kstR complex*, but at two points (77–92 and 149–172 residues) fluctuations are larger due to the presence of binding regions. In the presence of ligand with KstR protein, at two points, lower transitions were observed, and the system's overall compactness shows an increase after 11 *ns*. The difference in RMSF value (for both) to the endpoint of the simulation is 0.07 *nm*. This significant difference in the RMSF value of the native structure indicates that the ligand fits into the binding site.

Radius of gyration (Rg)

a) The radius of gyration (*Rg*) analysis of the *FurB* was carried out to determine the compactness of the protein system during the simulations. In the presence of ligand, the average *Rg* score was drastically reduced from 1.80 *rg* (native structure of FurB) to 1.59 *nm*. This complex underwent two drastic transitions which were observed from 1.60 *nm* to 1.40 *nm* and 1.40 *nm* to 1.55 *nm*, then the system was optimized after 15.4 *ns* at 1.5 *rg* (*nm*). The decrease in *Rg score* from the native structure points out that ligand binds into the binding cavity of the FurB.

b) In the presence of ligand with IdeR protein, the average *Rg* score was 0.06 *rg* decreased. A slight transition of 0.12 *nm* was spotted and after 12.6 *ns*, the system was optimized at 1.45 *rg* and the average difference in *rg score* at the end of both simulations was 0.11 *nm*. This significant difference in *Rg score* from the native structure points out that ligand binds into the binding site of the FurB.

c) In the case of RegX3, we observed structural fluctuations throughout the simulation, but in the case of *RegX3 complex* the amplitude of the fluctuations was smaller. The decrease in the transition of 0.487 *nm* occurred at 3.7 *ns*, but the system was optimized after 14.6 *ns* at 1.9 *nm*. However, the simulation finished with a total drift of 0.69 *nm* from the native structure and this difference indicates that the ligand binds into the RegX3 pocket.

d) In the presence of ligand with MosR, the average *Rg* score drastically decreases from 1.73 *nm* (native structure) to 1.35 *n*. This complex underwent structural fluctuations starting from first 0.17 *ns* to 5.29 *ns* and the compactness of the system increasing after 5.5 *ns* at 1.37 *nm*. This

difference indicates that the ligand binds to the active site of MosR.

e) In presence of ligand with KstR protein, at two points, lower transitions were observed, and the system's overall compactness witnessed an increase after 11 *n*. The difference in *rg score* (for both) to the endpoint of the simulation is 0.07 *nm*. This significant difference in *Rg score* from the native structure strongly indicates that the ligand binds to the active site of KstR.

Solvent accessible surface area

a) Solvent accessible surface area (SASA) remained relatively constant for the FurB protein at 73.68 nm^2, but in the case of FurB complex the pattern is different, SASA decreases from 73.20 nm^2 to 71 nm^2 and average fluctuation occurred near 70 nm^2 upto 10 *ns*. The system is optimized after 68.5 nm^2 at the 11 *ns* upto the endpoint of the simulation. The decrease in *SASA* caused by the change in protein conformation during its folding must be accompanied by the corresponding increase in the number of native contacts with the ligand, clearly indicating that ligand (*ZINC*03871613) binds into the active site of the FurB.

b) In the case of IdeR, we observed the structural fluctuations in SASA throughout the simulation, but these fluctuations diminish later on and the overall system is optimized after 79.5 but in the case of *IdeR complex* the pattern is different, the average *surface area* is drastically decreased from 71.78 nm^2 (native structure of IdeR) to 77.78 nm^2. The decrease in *SASA* strongly indicates that inhibitor (*ZINC*03871614) preferentially fits into the active site of IdeR.

c) In the case of RegX3, SASA remained stable up to 127.434 nm^2 at 8.5 *ns*, but the slight transition was observed at 7.183 nm^2, but in the case of *RegX*3 *complex* the pattern is different, the average surface area is slightly decreased from 123.75 nm^2 (native structure of IdeR) to 120.014 nm^2 and system is optimized after 6.68 *ns* at 119 nm^2. However, the simulation finished with a total drift off 10.209 nm^2 from the native structure and this difference in SASA indicates the ligand binding into the RegX3 pocket.

d) The SASA remained relatively constant for the MosR at 70.25 nm^2, but in the case of *FurB complex* the pattern is different; the SASA is decreasing from 69.59 nm^2 to below 62 nm^2, and therefore, systems compactness increases. The decrease in *SASA* strongly indicates that inhibitor (*ZINC*03871615) preferentially fits into the active site of MosR.

e) In the case of KstR protein and complex, gradual upper transition and lower transition were observed, respectively, but SASA remained relatively constant, and the overall system is optimized after 7.5 *ns* at 103 nm^2.

Network analysis and nodes characterization

The Protein-protein interaction (PPI) network was constructed using the five seed genes from the STRING database. In the present study, we considered only the immediate interacting partners (not more than 5 interactors) that abided the medium confidence score of 0.400. We have considered occurrence across the genome (suggesting that protein has a similar function or an occurrence in the same metabolic pathway further which to be expressed together and hold similar phylogenetic profile.), neighborhood (similar genomic context in different species suggesting similar functions of the proteins), putative homologs, gene fusions (that means proteins that are fused in some genomes are the most likely to be functionally linked), co-expression. We observed that FurB is present in the neighborhood of *MRA*_2382 and *Glys* and IdeR, KstR, Regx3, and MosR are in the neighborhood of *SigB*, *FadE*34, *SenX*3, and *Rv*1050 respectively, while RegX3 is fused with *PhoR*, *MtrB*, and *MtubH*3_010100022685. In the light, being a broad-spectrum antibiotics concept (i.e., designing multi-target drugs), it can be inferred from Tab. 2 that the interacting partners of RegX3 make it a most pliable target to any drug design for it. As homologs of RegX3's interacting partners are found co-expressed in other species of bacteria, it means it may be closely linked to MTB. In order to rank the targets based on their network interactions, KstR and RegX3 showcase highly influential interactions followed by MosR, IdeR, and FurB. The complete details of five seed genes and their interactions with other important genes are demonstrated in Fig. 6 and Tab. 2, which illustrates the PPI neighborhood of the 5 receptors (FurB, IdeR, KstR, RegX3, and MosR). The nodes of the graph represent proteins and the connections illustrate their known or predicted direct and indirect interactions.

Discussion

Till now TB has claimed the lives of millions of people across the world, despite our continuous efforts it is emerging as the next challenge for us to eradicate this ailment. Here we have tried to identify new scaffolds for drug discovery by repurposing FDA-approved drugs against *M. tuberculosis*. Almost all drugs repositioning concepts require at least some experimental validation of assessment for its efficacy, therefore we have adopted an *in-silico* approach to support experimental work in developing effective drugs in a shorter duration. Our systematic study has highlighted several important observations; molecular docking analysis of a set of 828 drugs with the best GoldScore ($\geq$ 55) were selected and out of which 11 drugs were frequently present within the top 20 GoldScore ranks and *ZINC03871613*, *ZINC03871614*, *ZINC03871615* are top scorer drugs. Hence, we consider all these 11 drugs as promising drugs as lead drugs for further research towards repurposing against TB.

The ROC curve applied to the retrospective analysis of a virtual screening experiment is a plot of the true positive fractions (TPR, y-axis) versus false positive fractions (FPR, x-axis) for all drugs in a ranked dataset. The ROC curve analysis reveals either perfect discrimination, i.e., passes through the upper left corner (100% sensitivity, 100% specificity), or defective discrimination. Therefore, the closer the ROC curve is to the upper left corner, the higher the overall accuracy of the test[58]. The area under the ROC curve (ROC AUC) outlines the overall performance thus higher the AUC, the higher is the accuracy. In this case, we

TABLE 2

Protein-Protein interaction: The evidence suggesting a functional link of proteins, including (a) Co-occurrence (b) Neighbourhood, (c) Putative homologs, (d) Gene fusions, (e) Co-expression

Interacted Protein	Co-occurrence (Score)	Intergenic distance (BP)	Putative Homologous (Score)	Neighbourhood (Score)	Not neighbourhood in the genome but homologous in other species (Score)	Gene Fusion (Score)	Co-expression (Score)	Putative homologs are co-expressed in other species (Score)
FurB								
FurA	0.611	NA	NA	NA	NA	NA	NA	NA
MRA_2382	NA	0 bp	NA	0.859	NA	NA	NA	NA
GlyS	NA	103524 bp	0.406	0.579	NA	NA	NA	NA
MRA_1920	0.611	NA	NA	NA	NA	NA	NA	NA
MRA_2383	0.782	NA	NA	NA	NA	NA	NA	NA
IdeR								
MRA_0086	NA	NA	0.612	NA	NA	NA	NA	NA
MRA_2739	0.782	NA	NA	NA	NA	NA	NA	NA
MtubH3_10100009904	0.651	NA	NA	NA	0.047	NA	NA	NA
sigB	NA	134 bp	NA	0.550	0.128	NA	NA	NA
KstR								
Rv3521	0.779	NA	NA	NA	0.047	NA	NA	0.050
Rv3542c	0.752	NA	NA	NA	0.047	NA	NA	0.058
fadE34	0.630	80.35*k* bp	NA	0.541	0.120	NA	NA	0.051
kshA	0.745	NA	NA	NA	NA	NA	NA	0.058
Rv0760c	0.769	NA	NA	NA	NA	NA	NA	NA
RegX3								
phoR	0.719	NA	0.415	NA	NA	0.001	0.075	0.075
senX3	0.764	229 bp	0.415	0.480	NA	NA	NA	0.075
mtrB	0.662	NA	0.415	NA	NA	0.002	0.086	0.075
prrB	0.665	NA	0.415	NA	NA	NA	0.083	0.132
MtubH3_010100022685	0.765	NA	0.415	NA	NA	0.002	NA	0.075
MosR								
narL [Rv0844c]	NA	NA	NA	NA	NA	NA	NA	0.058
Rv1364c	0.304	NA	NA	NA	NA	NA	NA	0.058
Rv0195	NA	NA	NA	NA	NA	NA	NA	0.058
devR	NA	NA	NA	NA	NA	NA	NA	0.058
Rv1050	NA	229 bp	NA	0.480	NA	NA	NA	NA

Note: Probabilistic values (0 to 1), Not Available (NA).

performed former experimentin order to identify the interaction capability of the targets with other potential based on the fitness value calculated using various parameters, e.g., interaction entropy. We found fitness values give a perfect discrimination, i.e., highly accurate, while interaction entropy contributes to the larger part of this perfection in each case (for both active and inactive ligands) as shown in ROC curve analysis of active and inactive ligands against targets in Fig. 7.

The protein-ligand complex with top-ranked drugs was used for the dynamics simulation study in order to see the effect of top scorer drugs on the structural stability of all five targets. It was found that these top scorer drugs preferentially fit into the active site of the targets. RMSD of all the protein's initial structures and protein-ligand complexes were calculated. Throughout the simulation period, significant drifts were observed in the backbone of FurB, IdeR, KstR, RegX3, and MosR and protein-ligand complexes, implying that binding of drug candidates at the active sites of the targets is not only preferentially fitting, but also disturbs the structure of proteins, i.e., the structure became more compact that is also proved by RG-score analysis (The lowest radius of

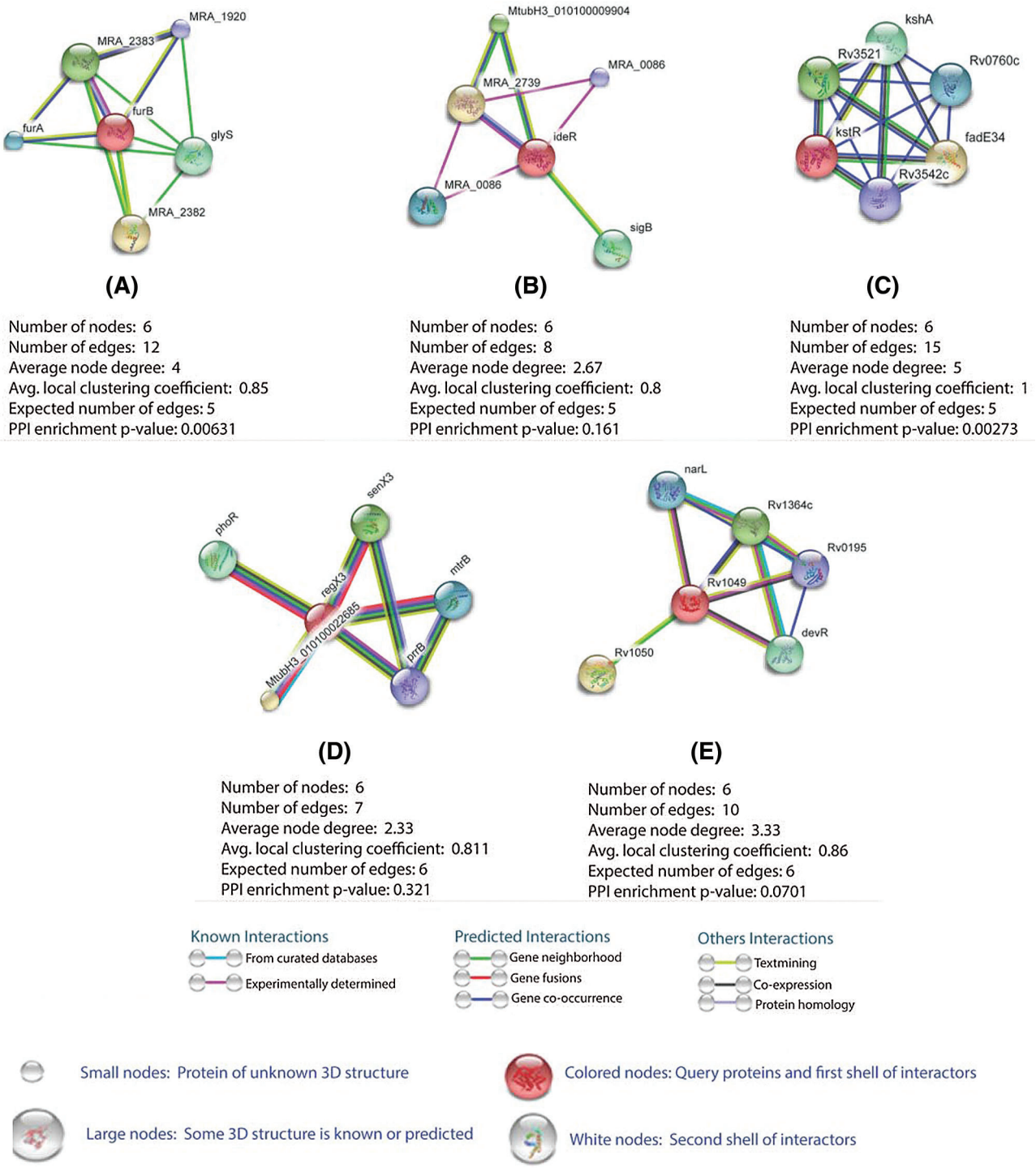

FIGURE 6. Analysis of protein-protein interaction (PPI) using STRING 10.5 server. The figure illustrates the PPI neighborhood of the 5 receptors (FurB, IdeR, KstR, RegX3, and MosR), the nodes of the graph represent proteins and the connections illustrate their known or predicted direct and indirect interactions. The connection between any two proteinnodes is based on the available information mined from relevant.

gyration mean more compact structure). RMSF analysis suggests that the observed residual fluctuations were largest in active sites of proteins that confirm the important role being played by these residues in the ligand-binding process. The significant drifts in native structures and protein-ligand complexes were observed in SASA analysis. The decrease in *SASA* caused by the change in protein conformation during its folding must be accompanied by the corresponding increase in the number of native contacts with ligand, clearly indicating that ligands tightly fit into the active sites. We performed hydrogen bond analysis and extracted the complex at the particular interval (5000, 10,000, 15,000, 20,000 ps, respectively) in the PDB format using g_h bond utility of GROMACS. However, we have noticed that one or two residues (that formed H-bonds from ligands) from each protein are common in all 4 intervals of time (5, 10, 15, 20 ns) that indicate that ligands are tightly bounds in the active sites. Apart from virtual screening and simulation

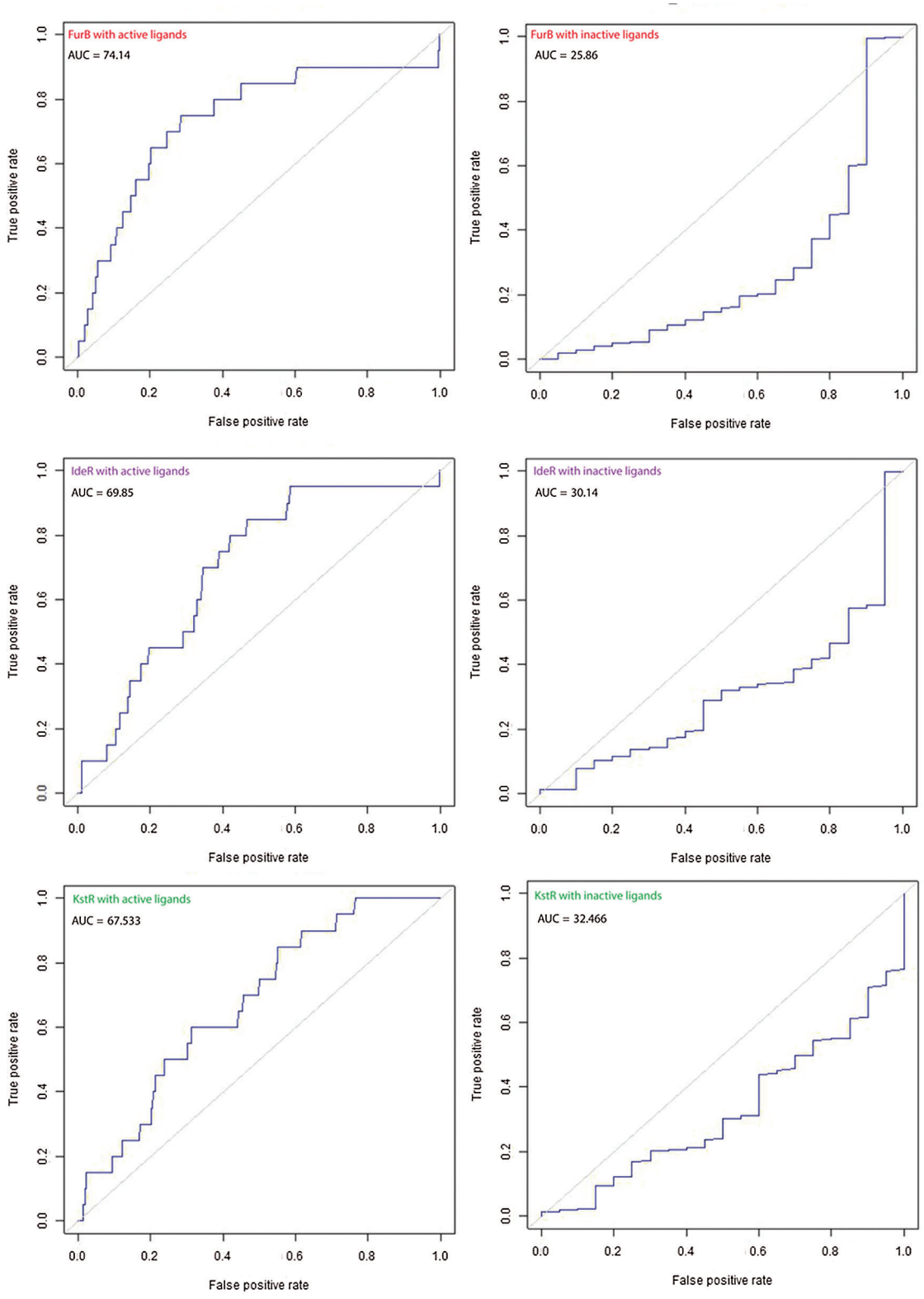

FIGURE 7. (continued)

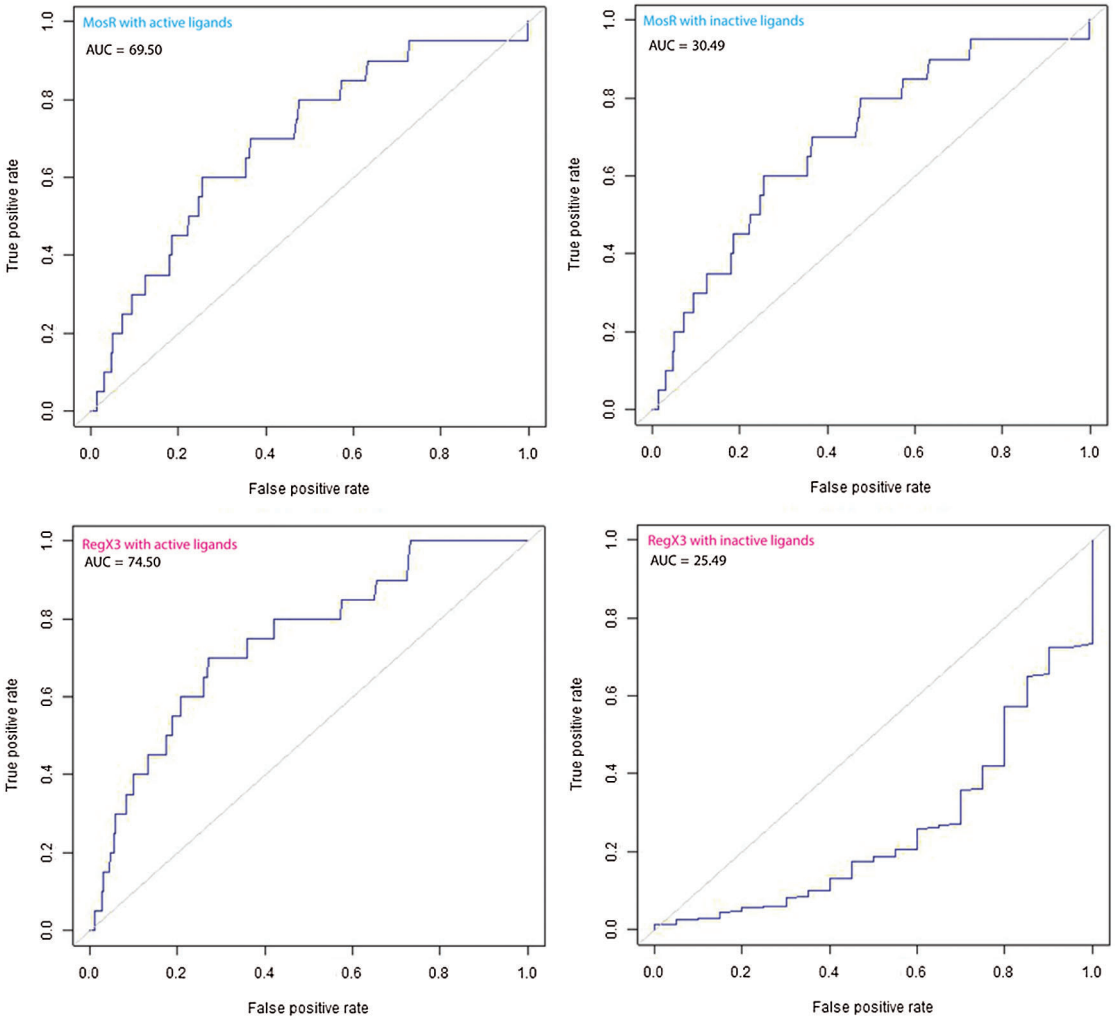

FIGURE 7. ROC curve analysis of active and inactive ligands against targets.

study, we analyzed the PPI network of target proteins to evaluate the functional genomics information and for providing an instinctive platform for annotating structural, functional, and evolutionary properties of proteins. For a better understanding of the effects of cellular interconnectedness on disease progression the analysis of PPI's may lead to the detection of disease genes and disease pathways, which may offer better targets for drug development. It has been clearly shown that the method utilized in this study is successful in finding out the most promising drug candidates against these targets that play a key role in the progression of TB disease. This work can be further explored to study the receptor-ligand interactions experimentally and assessment of their biological activity would help in specifying drugs against these key targets of MTB.

Conclusion

Tuberculosis (TB), being one of the major public health concerns, still lacks a complete and quick cure due to the *Mycobacterium tuberculosis* (MTB) strains resistant to existing drugs. Hence, it is important to look for new and effective drugs that can inhibit several putative drug targets. In this paper, we executed a computational drug repurposing pipeline to identify promising FDA-approved drugs against five key-regulatory genes of Mtb, namely, FurB, IdeR, KstR, MosR, and RegX3. Our study found 11 drug candidates including ZINC03871613, ZINC03871614, and ZINC03871615 as the top three drug candidates. In order to validate these results, a molecular dynamics simulation study was performed which indicates that inhibitors preferentially bind to the active site of the targets. This finding opensa new application domain in the form of anti-tuberculosis agents. This study can be further extended to explore the receptor-ligand interactions experimentally and assessment of their biological activity against key targets of MTB.

Availability of Data and Materials: Available on request to the authors.

Author Contribution: The idea was conceived by XY and KR, an experiment was designed by AA and KR, result analysis by AA, and the manuscript written by XY, AA, and KR. All authors reviewed the results and approved the final version of the manuscript.

Conflicts of Interest: The authors declare that they have no conflicts of interest to report regarding the present study.

References

Afzal O, Kumar S, Kumar R, Firoz A, Jaggi M, Bawa S (2014). Docking based virtual screening and molecular dynamics study to identify potential monoacylglycerol lipase inhibitors. *Bioorganic & Medicinal Chemistry Letters* **24**: 3986–3996.

Ahmad A, Cai Y, Chen X, Shuai J, Han A (2015). Conformational dynamics of response regulator RegX3 from Mycobacterium tuberculosis. *PLoS One* **10**: e0133389.

Ahmad F, Kumar S (2016). Rewiring of interconnected hubs in Gene Interaction Network of *Mycobacterium tuberculosis* and its survival in human host. *Journal of Applied Computing* **1**: 38–50.

Ahmad S (2011). Pathogenesis, immunology, and diagnosis of latent Mycobacterium tuberculosis infection. *Clinical and Developmental Immunology* **2011**: 814943.

Alam A, Ali S, Ahamad S, Malik MZ, Ishrat R (2016). From ZikV genome to vaccine: *in silico* approach for the epitope-based peptide vaccine against Zika virus envelope glycoprotein. *Immunology* **149**: 386–399.

Almatar M, Almandeal H, Var I, Kayar B, Köksal F (2017). New drugs for the treatment of *Mycobacterium tuberculosis* infection. *Biomedicine & Pharmacotherapy* **91**: 546–558.

Autiero I, Langella E, Saviano M (2013). Insights into the mechanism of interaction between trehalose-conjugated beta-sheet breaker peptides and Aβ (1-42) fibrils by molecular dynamics simulations. *Molecular BioSystems* **9**: 2835–2841.

Banerjee S, Farhana A, Ehtesham NZ, Hasnain SE (2011). Iron acquisition, assimilation and regulation in mycobacteria. *Infection, Genetics and Evolution* **11**: 825–838.

Berman HM, Westbrook J, Feng Z, Gilliland G, Bhat TN et al. (2000). The protein data bank. *Nucleic Acids Research* **28**: 235–242.

Bjelkmar P, Larsson P, Cuendet MA, Hess B, Lindahl E (2010). Implementation of the CHARMM force field in GROMACS: Analysis of protein stability effects from correction maps, virtual interaction sites, and water models. *Journal of Chemical Theory and Computation* **6**: 459–466.

Brugarolas P, Movahedzadeh F, Wang Y, Zhang N, Bartek IL et al. (2012). The oxidation-sensing regulator (MosR) is a new redox-dependent transcription factor in Mycobacterium tuberculosis. *Journal of Biological Chemistry* **287**: 37703–37712.

Carroll P, Faray-Kele MC, Parish T (2011). Identifying vulnerable pathways in *Mycobacterium tuberculosis* by using a knockdown approach. *Applied and Environmental Microbiology* **77**: 5040–5043.

Cau Y, Valensin D, Mori M, Draghi S, Botta M (2018). Structure, function, involvement in diseases and targeting of 14-3-3 proteins: An update. *Current Medicinal Chemistry* **25**: 5–21.

Cheatham T, Miller J, Fox T, Darden T, Kollman P (1995). Molecular dynamics simulations on solvated biomolecular systems: The particle mesh Ewald method leads to stable trajectories of DNA, RNA, and proteins. *Journal of the American Chemical Society* **117**: 4193–4194.

Chou KC, Mao B (1988). Collective motion in DNA and its role in drug intercalation. *Biopolymers: Original Research on Biomolecules* **27**: 1795–1815.

De Azevedo Jr WF, Canduri F, Fadel V, Teodoro LG, Hial V et al. (2001). Molecular model for the binary complex of uropepsin and pepstatin. *Biochemical and Biophysical Research Communications* **287**: 277–281.

De Azevedo WF (2011). Molecular dynamics simulations of protein targets identified in *Mycobacterium tuberculosis*. *Current Medicinal Chemistry* **18**: 1353–1366.

Dua K, Rapalli VK, Shukla SD, Singhvi G, Shastri MD et al. (2018). Multi-drug resistant Mycobacterium tuberculosis & oxidative stress complexity: Emerging need for novel drug delivery approaches. *Biomedicine & Pharmacotherapy* **107**: 1218–1229.

García JL, Uhía I, Galán B (2012). Catabolism and biotechnological applications of cholesterol degrading bacteria. *Microbial Biotechnology* **5**: 679–699.

Heberlé G, De Azevedo WF (2011). Bio-inspired algorithms applied to molecular docking simulations. *Current Medicinal Chemistry* **18**: 1339–1352.

Ho NAT, Dawes SS, Crowe AM, Casabon I, Gao C et al. (2016). The structure of the transcriptional repressor KstR in complex with CoA thioester cholesterol metabolites sheds light on the regulation of cholesterol catabolism in Mycobacterium tuberculosis. *Journal of Biological Chemistry* **291**: 7256–7266.

India TB Report (2018). Ministry Of Health and Family Welfare.

Irwin JJ, Sterling T, Mysinger MM, Bolstad ES, Coleman RG (2012). ZINC: A free tool to discover chemistry for biology. *Journal of Chemical Information and Modeling* **52**: 1757–1768.

Johansson MU, Zoete V, Michielin O, Guex N (2012). Defining and searching for structural motifs using DeepView/Swiss-PdbViewer. *BMC Bioinformatics* **13**: 173.

Jones G, Willett P, Glen RC (1995). Molecular recognition of receptor sites using a genetic algorithm with a description of desolvation. *Journal of Molecular Biology* **245**: 43–53.

Jones G, Willett P, Glen RC, Leach AR, Taylor R (1997). Development and validation of a genetic algorithm for flexible docking. *Journal of Molecular Biology* **267**: 727–748.

Karaman B, Sippl W (2019). Computational drug repurposing: Current trends. *Current Medicinal Chemistry* **26**: 5389–5409.

Karthick V, Ramanathan K (2013). Virtual screening for oseltamivir-resistant a (H5N1) influenza neuraminidase from traditional Chinese medicine database: A combined molecular docking with molecular dynamics approach. *Springerplus* **2**: 115.

Kendall SL, Burgess P, Balhana R, Withers M, Ten Bokum A et al. (2010). Cholesterol utilization in mycobacteria is controlled by two TetR-type transcriptional regulators: kstR and kstR2. *Microbiology* **156**: 1362.

Khalid Z, Ahmad S, Raza S, Azam SS (2018). Subtractive proteomics revealed plausible drug candidates in the proteome of multi-drug resistant *Corynebacterium diphtheriae*. *Meta Gene* **17**: 34–42.

King-Scott J, Nowak E, Mylonas E, Panjikar S, Roessle M et al. (2007). The structure of a full-length response regulator from Mycobacterium tuberculosis in a stabilized three-dimensional domain-swapped, activated state. *Journal of Biological Chemistry* **282**: 37717–37729.

Krueger J, Thiel P, Merelli I, Grunzke R, Gesing S (2016). Portals and web-based resources for virtual screening. *Current Drug Targets* **17**: 1649–1660.

Lanza V, Milardi D, Di Natale G, Pappalardo G (2018). Repurposing of copper (II)-chelating drugs for the treatment of neurodegenerative diseases. *Current Medicinal Chemistry* **25**: 525–539.

Li MS, Monahan IM, Waddell SJ, Mangan JA, Martin SL et al. (2001). cDNA-RNA subtractive hybridization reveals increased expression of mycocerosic acid synthase in intracellular Mycobacterium bovis BCG. *Microbiology* **147**: 2293–2305.

Lin SX, Lapointe J (2013). Theoretical and experimental biology in one—A symposium in honour of Professor Kuo-Chen Chou's 50th anniversary and Professor Richard Giegé's 40th anniversary of their scientific careers. *Journal of Biomedical Sciences and Engineering* **06**: 435–442.

Lucarelli D, Russo S, Garman E, Milano A, Meyer-Klaucke W, Pohl E (2007). Crystal structure and function of the zinc uptake regulator FurB from *Mycobacterium tuberculosis*. *Journal of Biological Chemistry* **282**: 9914–9922.

Morrone Xavier M, Sehnem Heck G, Boff De Avila M, Maria Bernhardt Levin N, Oliveira Pintro V et al. (2016). SAnDReS a computational tool for statistical analysis of docking results and development of scoring functions. *Combinatorial Chemistry & High Throughput Screening* **19**: 801–812.

Palos I, Lara-Ramirez EE, Lopez-Cedillo JC, Garcia-Perez C, Kashif M et al. (2017). Repositioning FDA drugs as potential cruzain inhibitors from Trypanosoma cruzi: Virtual screening, *in vitro* and *in vivo* studies. *Molecules* **22**: 1015.

Panina EM, Mironov AA, Gelfand MS (2003). Comparative genomics of bacterial zinc regulons: Enhanced ion transport, pathogenesis, and rearrangement of ribosomal proteins. *Proceedings of the National Academy of Sciences of the United States of America* **100**: 9912–9917.

Pei JF, Qi N, Li YX, Wo J, Ye BC (2021). RegX3-mediated regulation of methylcitrate cycle in *Mycobacterium smegmatis*. *Frontiers in Microbiology* **12**: 119.

Peters JS, Ismail N, Dippenaar A, Ma S, Sherman DR et al. (2020). Genetic diversity in Mycobacterium tuberculosis clinical isolates and resulting outcomes of tuberculosis infection and disease. *Annual Review of Genetics* **54**: 511–537.

Pohl E, Holmes RK, Hol WG (1999). Crystal structure of the iron-dependent regulator (IdeR) from *Mycobacterium tuberculosis* shows both metal binding sites fully occupied. *Journal of Molecular Biology* **285**: 1145–1156.

Potemkin V, Grishina M (2018). Grid-based technologies for in silico screening and drug design. *Current Medicinal Chemistry* **25**: 3526–3537.

Qazi S, Raza K (2021). Phytochemicals from Ayurvedic plants as potential medicaments for ovarian cancer: An *in silico* analysis. *Journal of Molecular Modeling* **27**: 114.

Rester U (2008). From virtuality to reality-Virtual screening in lead discovery and lead optimization: A medicinal chemistry perspective. *Current Opinion in Drug Discovery & Development* **11**: 559–568.

Roberts G, Vadrevu IS, Madiraju MV, Parish T (2011). Control of CydB and GltA1 expression by the SenX3 RegX3 two component regulatory system of Mycobacterium tuberculosis. *PLoS One* **6**: e21090.

Rohilla A, Khare G, Tyagi AK (2017). Virtual Screening, pharmacophore development and structure based similarity search to identify inhibitors against IdeR, a transcription factor of *Mycobacterium tuberculosis*. *Scientific Reports* **7**: 4653.

Rollinger JM, Stuppner H, Langer T (2008). Virtual screening for the discovery of bioactive natural products. *Natural Compounds as Drugs* **I**: 211–249.

Sanz J, Navarro J, Arbués A, Martín C, Marijuán PC et al. (2011). The transcriptional regulatory network of Mycobacterium tuberculosis. *PLoS One* **6**: e22178.

Savoia D (2016). New antimicrobial approaches: Reuse of old drugs. *Current Drug Targets* **17**: 731–738.

Singh P, Jaiyeola B, Kerru N, Ebenezer O, Bissessur A (2017). A review of recent advancements in anti-tubercular molecular hybrids. *Current Medicinal Chemistry* **24**: 4180–4212.

Snel B, Lehmann G, Bork P, Huynen MA (2000). STRING: A web-server to retrieve and display the repeatedly occurring neighbourhood of a gene. *Nucleic Acids Research* **28**: 3442–3444.

van der Spoel D, Lindahl E, Hess B, Groenhof G, Mark AE, Berendsen HJ (2005). GROMACS: Fast, flexible, and free. *Journal of Computational Chemistry* **26**: 1701–1718.

Wang Q, Canutescu AA, Dunbrack RL, Jr (2008). SCWRL and MolIDE: Computer programs for side-chain conformation prediction and homology modeling. *Nature Protocols* **3**: 1832.

Ward SK, Abomoelak B, Marcus S, Talaat AM (2010). Transcriptional profiling of *Mycobacterium tuberculosis* during infection: Lessons learned. *Frontiers in Microbiology* **1**: 121.

Weiner J, Domaszewska T, Donkor S, Kaufmann SH, Hill PC, Sutherland JS (2020). Changes in transcript, metabolite, and antibody reactivity during the early protective immune response in humans to *Mycobacterium tuberculosis* infection. *Clinical Infectious Diseases* **71**: 30–40.

Zoete V, Cuendet MA, Grosdidier A, Michielin O (2011). SwissParam: A fast force field generation tool for small organic molecules. *Journal of Computational Chemistry* **32**: 2359–2368.

Supplementary Table S1

List of docking results at the set threshold of 55 Gold score: FurB was docked with 111, IdeR was docked with 355, KstR was docked with 193, MosR was docked with 157, and RegX3 was docked with 12 out of 1985 compounds.